energy&fuels

pubs.acs.org/EF Article

Kinetics of Gas Phase CO_2 Adsorption on Bituminous Coal from a Shallow Coal Seam

Sivachidambaram Sadasivam,* Shakil Masum, Min Chen, Kamil Stańczyk, and Hywel Thomas

Cite This: *Energy Fuels* 2022, 36, 8360–8370

Read Online

ACCESS | Metrics & More | Article Recommendations

ABSTRACT: This article examines the CO_2 adsorption–desorption kinetics of bituminous coal under low pressure injection (0.5 MPa) in the context of CO_2 sequestration in shallow level coal seams. This study used two different sizes of intact core samples of bituminous samples from seam no. 30 at the Experimental Mine Barbara (EMB) in Katowice, Poland. Manometric adsorption kinetics experiments were conducted on 50 mm dia. 60 mm long coal core samples (referred to as EMB1) and 50 mm dia. 30 mm long coal core samples (referred to as EMB2). The kinetics of adsorption at injection pressures ranging from 0.1 to 0.5 MPa were compared to those at elevated pressures ranging from 0.5 to 4.5 MPa. For the first time, intact sample adsorption–desorption data were fitted in pseudo first order (PFO), pseudo second order (PSO), and Bangham pore diffusion models. The PSO model fits the data better than the PFO model, indicating that bulk pore diffusion, surface interaction, and multilayer adsorption are the rate-determining steps. Comparing the equilibrium amount of adsorbed (q_e) obtained for the powdered samples (9.06 g of CO_2/kg of coal at 0.52 MPa) with intact samples (11.68 g/kg at 0.53 MPa and 7.58 g/kg at 0.52 MPa for the intact EMB1 and EMB2 samples) showed the importance of conducting experiments with intact samples. The better fit obtained with the Bangham model for lower pressure equilibrium pressures (up to 0.5 MPa) compared to higher pressure equilibrium pressures (4.5 MPa) indicates that bulk pore diffusion is the rate-determining step at lower pressures and surface interaction takes over at higher pressures. The amount of CO_2 trapped within the coal structure following the desorption experiments strengthens the case for intact bituminous coal samples' pore trapping capabilities.

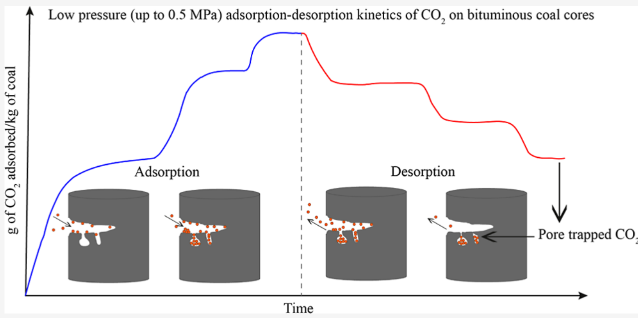

1. INTRODUCTION

CO_2, along with other greenhouse gases, is the primary contributor to global warming. Accumulative emissions of CO_2 are estimated to be 2035 ± 205 Gt of CO_2 and increasing at the current emission rate of 40 Gt CO_2/year.[1,2] Carbon capture and sequestration (CCS) in geological media is viewed as a promising option for limiting the adverse effects of climate change. Deep saline aquifer sequestration, mineralization with rocks, and coal seam sequestration all seem to be viable options for carbon sequestering. Countries were urged to speed up the phaseout of coal use by 2030 in order to limit the temperature increase <1.5 °C preferably by the end of the century.[3−6] CCS in coal might be a practical option for the effective use of un-mineable coal seams.[7]

Coal is a fractured and porous structured carbonous material found in different ranks such as lignite, subbituminous, bituminous, and anthracite depending on the coalification process. The coal's ability to adsorb gas demonstrates its applicability for CCS operations. Adsorption of methane in coal seams is facilitated by the high surface area and porous nature of the coal.[8,9] According to studies, the coal surface has a stronger affinity for CO_2 than that for CH_4, especially in bituminous coal samples.[10−14]

CO_2 trapping in coal is influenced by several factors, including sequestration capacity, gas permeability/injectivity, pressure, temperature, coal swelling behavior, confinement pressure, moisture content, and depth.[9,15,16] According to the gas physical adsorption phenomenon, increasing the equilibrium pressure increased the CO_2 adsorption capacity of coal. The sorption isotherm, on the other hand, showed decreasing trends at pressures near and above the critical pressures (7.38 MPa at a temperature of 304.1 K).[17−21] Typically, the reported adsorption capacity increased with the decrease in temperature,[22] and the majority of the current literature reported the adsorption isotherm obtained at higher temperatures (308.15,

Received: May 6, 2022
Revised: June 29, 2022
Published: July 18, 2022

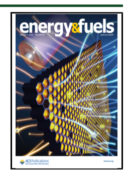

https://doi.org/10.1021/acs.energyfuels.2c01426
Energy Fuels 2022, 36, 8360–8370

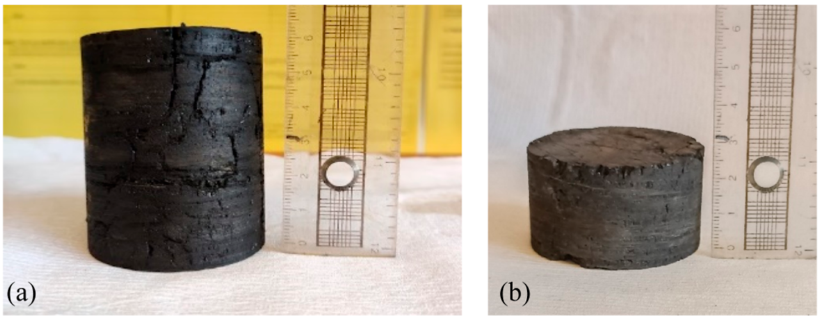

Figure 1. Core samples of bituminous coal cores extracted from large coal blocks. (a) EMB1: 50 mm dia. and 60 mm length, (b) EMB2: 50 mm dia. and 30 mm length.

318.15, 328.15, and 377.15 K).[23,24] However, there is very limited for the CO_2 adsorption on coal at lower temperatures (298.15 and 290.15 K).[25,26]

In general, coal seam depths of less than 1000 m are preferred for CO_2 sequestration. Deeper than 1000 m, the confining pressure may affect coal permeability, eventually reducing the injectivity and CO_2 adsorption capacity.[27] Shallower than 1000 m depth, where the temperature and pressure are expected to be less than the critical parameters of CO_2 (31 °C and 7.38 MPa). The subcritical temperature and pressure adsorption behavior of CO_2 is currently understood to a lesser extent.[7] Most studies have used powdered coal specimens to study adsorption capacity and kinetics, with very limited data on intact samples.[28,29] To understand the CO_2 trapping capabilities of bituminous coal at subcritical pressure and temperature, it is critical to conduct comprehensive adsorption−desorption experimental studies on large intact samples.

The CO_2 adsorption capacity of coal is correlated to its swelling behavior, and matrix swelling creates a pathway for CO_2 to permeate the coal's microfractures and nanopores.[25] The reversibility of trapped CO_2 in the pores is critical for estimating the coal seam's residual CO_2 retaining capacity. This parameter can be determined by examining the adsorption−desorption kinetics and hysteresis patterns. As such, a positive deviation in the hysteresis indicates that the adsorbate gas is not readily released to its equilibrium pressure and temperature values.[22] The kinetics of CO_2 desorption from coal has received less attention. Until now, it has been reported that a large proportion of CO_2 gas molecules are trapped in the structure of bituminous coal during the desorption process.[10] Previously, manometric experimental setups were used to examine the CO_2 adsorption kinetics of powdered samples of bituminous and anthracite coal at 35, 45, and 55 °C, as well as pressures up to 25 MPa.[23] Similarly, the spontaneity of CO_2 reversibility from the coal's nanopores can be explored by conducting adsorption−desorption kinetics studies with an intact specimen of porous bituminous coal under subcritical CO_2 conditions.

The pseudo-first-order (PFO) kinetic model and pseudo-second-order (PSO) kinetics have been widely applied for predicting the gas phase adsorption of CO_2 on coal.[30−34] The equilibrium amount of CO_2 adsorbed on an intact bituminous coal specimen obtained using the manometric method at pressure ranges up to 5 MPa and temperatures of 298.15, 308.15, and 318.15 K were shown to be in good agreement with the PSO model.[35] The rate-determining factor of adsorption was determined as the pore diffusion/condensation of CO_2. The PSO model assumes that the CO_2 adsorption on bituminous coal is dominated by surface interaction and bulk diffusion.[30] Nevertheless, the desorption kinetics of the intact specimen holds the key information on the rate-determining factor and most important to know the residual amount of CO_2 remaining in the coal seam. Bangham and Burt (1924, 2002)[36,37] successfully applied a kinetic model from the CO_2 adsorption experiments conducted on glass and Bangham and Sever (1925)[38] extended the pore diffusion model to the van der Waals adsorption of gases, which were well fitted with the model. Probing the rate-determining steps at low pressure injection would highlight the prominent adsorption mechanisms at low pressure injection at shallow depth coal seams.

From the current understanding, the limitation of available desorption kinetic data from the large bituminous sample at subcritical CO_2 conditions, investigation needs to be carried out to substantiate the candidature of shallow level coal seams as CCS reservoirs. Moreover, the gas phase adsorption of CO_2 at low injection pressure, reversibility, and residual CO_2 retained in the pores are the crucial information for shallow level sequestration, which has been less understood. Especially, the experimental studies[39] conducted in the subcritical range showed very limited data representing the pressure range below 0.5 MPa to ascertain the CO_2 behavior at these pressure ranges. A large number of studies have been conducted at the supercritical pressure range aiming to inject CO_2 in coal seams located below 1000 m assuming that environmentally safe, CO_2 can be stored at higher volume at high density. However, laboratory conditions cannot be replicated in the field and CO_2 can escape to different pressure and temperature regions in the ground. Moreover the higher confining pressure at deeper coal seams would affect the injectivity of CO_2.[40,41] Therefore, the current study attempted a detailed adsorption−desorption kinetic study of gas phase adsorption for shallow level injection. The shallow level of CO_2 storage required low pressure injection of gas phase CO_2 owing to the low confining pressures. The present study demonstrates the experimentally observed adsorption−desorption kinetics of CO_2 adsorption on large cores of bituminous coal samples at low pressure injections (less than 0.5 MPa) and at a temperature of 298.15 K obtained using a manometric adsorption apparatus. The data were fitted into PFO, PSO, and Bangham models to predict the rate-determining factors of adsorption and desorption processes.

2. MATERIALS AND METHODS

The bituminous coal specimens have been procured from the "seam-310" located at 30 m depth in Experimental Mine Barbara (hereafter referred to as EMB), at the Central Mining Institute, Katowice,

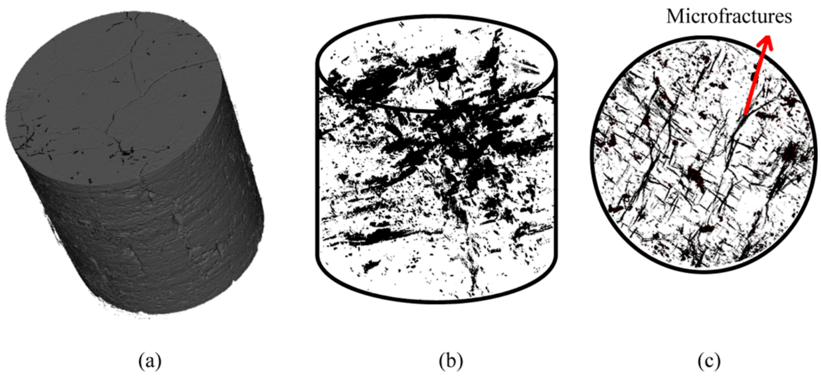

Figure 2. X-CT image reconstruction (a) and visualization of microfracture features (b,c; dark shades show the microfracture volume) in intact bituminous coal cores.

Poland. A core drilling machine with a drilling bit with a diamond saw tip (50 mm internal diameter) was employed to extract core samples of 50 mm dia. 60 mm length (referred to as EMB1) and 50 mm dia. 30 mm length samples (referred to as EMB2) (Figure 1). Ground pulverized coal was passed through a 63 μm mesh to obtain powdered coal samples.

The large-sized adsorbent was characterized for its microfracture network using X-ray computed tomography (X-CT) (Figure 2). The scans were used to quantify the microfractures and not the pores. The microfractures are separated from the matrix, and the volume of these flow paths (connected and unconnected fracture network) is quantified to compare with the He-pycnometry method. The images of the physical structure of the coal core adsorbent showed the unconnected fracture network volume which will become available to CO_2 owing to the swelling behavior of bituminous coal as described in previous studies.[42−45] The connected and unconnected void volume was about 1.5% of the bulk sample. Even though the volume was a negligible addition to the adsorption cell void volume (v_d; see Section 2.1), the v_d was adjusted with the excess volume measured by X-CT to calculate the molar volume of the adsorbed phase.

Proximate and ultimate analysis of EMB coal showed a moisture content of 7.54 and 6.39%, respectively, for the "as received" and "analytical" samples. The carbon content is 71.5% (approx.), the maximum ash content is 15.56%, and the vitrinite's reflectance is 0.57 ± 0.03%. The coal is classified as low rank bituminous coal. Table 1 summarizes the properties of the coal samples.

Table 1. Proximate and Ultimate Analysis of the EMB Coal Specimen[a]

parameter	value
As Received	
moisture (%)	7.54
ash (%)	15.56
S total (%)	0.51
calorific value (kJ/kg)	21 708
Analytical	
moisture W^a (%)	6.39
ash A^a (%)	16.52
volatile matter V^a (%)	33.94
calorific value A^a (kJ/kg)	23 019
C^a (%)	71.5
H^a (%)	3.70
N^a (%)	0.87
S^a total (%)	0.54
$S_c{}^a$ (%)	0.54
O^a (%)	14.03
vitrinite reflectance	0.57 ± 0.03%

[a]Oxygen calculated as follows: $(O^a) = 100 - (W^a) - (A^a) - (C^a) - (H^a) - (S_c{}^a) - (N^a)$ %.

2.1. Measurement of CO_2 Adsorption Kinetics by Manometric/Volumetric Method.

A manometric gas adsorption cell was employed to determine the CO_2 adsorption capacity of the core samples. The schematic of the apparatus and experimental setup is presented in Figure 3. The apparatus was designed and installed by GDS Instruments UK. A detailed description of the experimental setup is available at Mosleh (2014).[46]

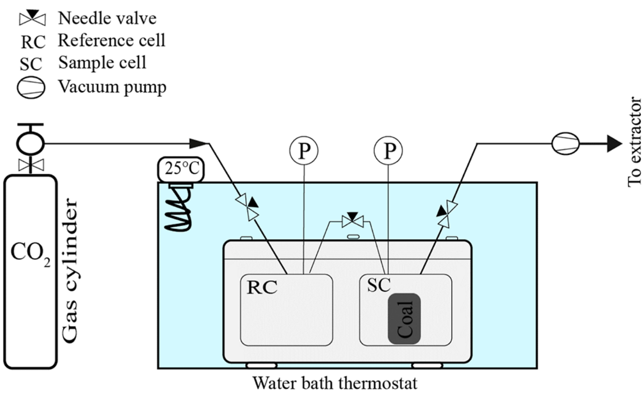

Figure 3. Schematic of the manometric gas adsorption cell and experimental setup.

To measure CO_2 adsorption in a manometric cell, a known amount of gas ($n_i^{CO_2}$) is injected into the reference cell (RC) and expanded into the sample cell (SC), which contains a coal sample that is degassed prior to the test using a vacuum pump attached to the adsorption cell (each sample was degassed for 24 h) (Figure 3). The amount of gas ($n_i^{CO_2}$) injected in the RC was calculated using the perfect gas law (eq 1) by precisely measuring the available volume for gas (v_{rc}) in the adsorption cell, pressure (p), and temperature (T). The volumes of adsorption cells were measured using the He-pycnometry method.[47] The pressure was measured using two pressure transducers connected to RC and SC (Figure 3). With time, the CO_2 gas pressure injected in the adsorption cell reduces because the gas molecules continue to adsorb on the adsorbents (coal). At a given time (t), the difference between the amount injected ($n_i^{CO_2}$) and the amount remaining in the gas phase ($n_e^{CO_2}$) is recorded as the amount of CO_2 adsorbed or desorbed ($q_{t,ad}^{CO_2}$) on the coal specimens. Once the equilibrium is attained, the pressure in the RC is progressively increased for the next pressure step up stages (the pressure ranges are given in Table 2), and the aforementioned procedures are repeated to calculate the cumulative amount of adsorbed CO_2 corresponding to the thermodynamic equilibrium pressure at a given time. After completing the adsorption test steps, pressure in the RC is progressively reduced and the amount of desorbed CO_2 is determined. In this experiment, the pressure values were recorded

https://doi.org/10.1021/acs.energyfuels.2c01426
Energy Fuels 2022, 36, 8360−8370

Table 2. CO_2 Adsorption−Desorption Experimental Program

experiment no.	sample	conditions	tests
EXP1	EMB1: 50 mm dia. × 60 mm length	0.5−4 MPa, 298 K	CO_2 adsorption
		3.6−0.085 MPa, 298 K	CO_2 desorption
EXP2		0.1−0.5 MPa, 298 K	CO_2 adsorption
		0.41−0.041 MPa	CO_2 desorption
EXP3	EMB2: 50 mm dia. × 30 mm length	0.1−0.4 MPa, 298 K	CO_2 adsorption
		0.37−0.38 MPa	CO_2 desorption
EXP4	powder (<63 μm)	0.1−0.5 MPa	CO_2 adsorption

every 10 s using a data logger. The equilibrium pressure was defined as a pressure value that remained steady for at least 4 h. The selected data points were used for calculating the adsorbed amount of CO_2 ($q_{t,ad/de}^{CO_2}$) at a time (t) during adsorption or desorption by employing the following equations[48−52]

$$n_i^{CO_2} = \frac{p^{CO_2} M v_{rc}}{RTZ_{(p,v)}};\quad n_t^{CO_2} = \frac{p_{eq}^{CO_2} M v_d}{RTZ_{(p,v)}} \tag{1}$$

$$q_{t,ad}^{CO_2} = \frac{n_t^{CO_2} - n_i^{CO_2}}{m_s} \quad \text{amount adsorbed during adsorption} \tag{2}$$

$$q_{t,de}^{CO_2} = \frac{n_i^{CO_2} - n_t^{CO_2}}{m_s} \quad \text{amount adsorbed during desorption} \tag{3}$$

where $q_{t,ad/de}^{CO_2}$ is the mass of CO_2 adsorbed on coal (g of CO_2/kg of coal) at time t during adsorption or desorption; $p_{eq}^{CO_2}$ is the equilibrium pressure of CO_2 (Pa); R is the universal gas constant (R = 8.314 Pa·m^3/K/mol); and M is the molar mass of CO_2 (M = 44.01 g/mol). v_d is the void volume available for gas (m^3), the available void volume for gas (V_d) in the RC and SC is approximated by He-pycnometry method,[47] Z is the compressibility factor of CO_2 which is calculated using cubic form of Peng−Robinson equation of state,[53] $n_i^{CO_2}$ is the known amount present in the gas phase at beginning of the adsorption experiment (g of CO_2), and $n_t^{CO_2}$ is the amount of CO_2 at the gas phase at time t.

Adsorption experiments were conducted using two different sizes of EMB coal core samples, 50 mm dia. 60 mm length (referred to as EMB1; Table 2) and 50 mm dia. 30 mm length (referred to as EMB2; Table 2) samples, at an injection pressure range of 0.1−0.5 MPa. The experiments were termed EXP2 and EXP3 for EMB1 and EMB2, respectively. The pressure range was chosen to comprehend the adsorption process of CO_2 injection at a low pressure in a shallow level coal seam with low confining stresses (an approximate vertical stress of 0.51− 0.7 MPa is expected at 30 m depth). One sample with a 50 mm dia. 60 mm length (EMB1) was tested at an intermediate pressure range of 0.5−4.5 MPa (termed as EXP1; Table 2) to compare the kinetics of the adsorption process at elevated pressure range in the subcritical range. The adsorption kinetics process of the large cores was compared with a powdered sample (termed as EXP4; Table 2). The experimental conditions are outlined in Table 2.

2.2. Kinetic Models. Adsorption kinetics data acquired from the experiments were fitted into the PFO and PSO rate eqs 4 and 5 to ascertain the rate-determining steps in CO_2 adsorption on EMB coal.[54,55]

$$\text{PFO:}\quad q_t = q_e(1 - e^{-k_{a1}t}) \tag{4}$$

$$\text{PSO:}\quad q_t = \frac{t}{\frac{1}{q_e}t + \frac{1}{k_{a2}q_e^2}} \tag{5}$$

where q_t = mass adsorbed per mass of adsorbent at time t (g of CO_2/kg of coal), q_e = mass adsorbed per mass of adsorbent at equilibrium, g of CO_2/kg of coal, k_{a1} = first-order rate constant for adsorption, h^{-1}, and k_{a2} = second-order rate constants for adsorption, kg/g h.

The PFO and PSO models have not so far been modeled for the desorption kinetics of CO_2 from coal. The current study adopts the desorption kinetic models proposed by Njikam and Schiewer (2012),[56] in which the adsorbate concentration remaining in the adsorbent during the desorption is the rate-determining factor (eqs 6 and 7).

$$\text{PFO:}\quad q_t = q_e/e^{k_{d1}t} \tag{6}$$

$$\text{PSO:}\quad q_t = \frac{q_e}{(1 + (k_{d2}q_e t))} \tag{7}$$

where q_t = mass adsorbed per mass of adsorbent at time t, g of CO_2/kg of coal, q_e = mass adsorbed per mass of adsorbent at the time of equilibrium, g of CO_2/kg of coal, k_{d1} = first-order rate constant for desorption, h^{-1} and k_{d2} = second-order rate constants for desorption, kg/g h.

The best fitting model was validated by the coefficient of determination (R^2) combined with the standard error of the estimate (eq 8).

$$\text{Standard error of estimate (SEOE)} = \sqrt{\left[\frac{\sum (q_{obs} - q_{fit})^2}{n}\right]} \tag{8}$$

where q_{obs} is the experimentally observed mass of CO_2 adsorbed at time t (g of CO_2/kg of coal), q_{fit} is the predicted mass of CO_2 adsorbed at time t (g of CO_2/kg of coal) by PFO or PSO models, and n is the number of experimental observations.

Bangham model have been used to predict the influence of the pore diffusion, the slowest step of the gas adsorption (eq 9).[39,57]

$$q_t = q_e(1 - \exp(-k_b t^n)) \tag{9}$$

where q_t is the mass adsorbed per mass of adsorbent at time t (g of CO_2/kg of coal), q_e is the mass adsorbed per mass of adsorbent at the time of equilibrium, g of CO_2/kg of coal, and k_b (h^{-1}) and n are constants of the model.

3. RESULTS AND DISCUSSION

The amount of CO_2 adsorbed−desorbed per kg of coal is calculated using eqs 2 and 3, respectively, for each pressure step of the adsorption and desorption experiments described earlier. The PFO, PSO, and Bangham models were fitted to the experimental data and to determine the rate-determining steps in CO_2 adsorption on intact bituminous coal.

3.1. Analysis of CO_2 Adsorption−Desorption Kinetics Data. The results of the PFO and PSO model fits to the kinetics data are presented in Figures 4−7 and the summary of the fitting exercises is in Tables 3−6. Overall, the PSO model fits the data better than the PFO model. The PSO model assumes that available surface and pore volume are driving factors and diffusion, or chemisorption/surface interaction, are the primary rate-determining steps. In Figures 4−6, the experimental results of adsorption kinetics are plotted against the PFO and PSO models for intact core samples (EXP1, EXP2, and EXP3), and the model parameters are listed in Tables 3−5. The R^2 values combined with the standard error of estimate indicate that the PSO model adequately describes

https://doi.org/10.1021/acs.energyfuels.2c01426
Energy Fuels 2022, 36, 8360−8370

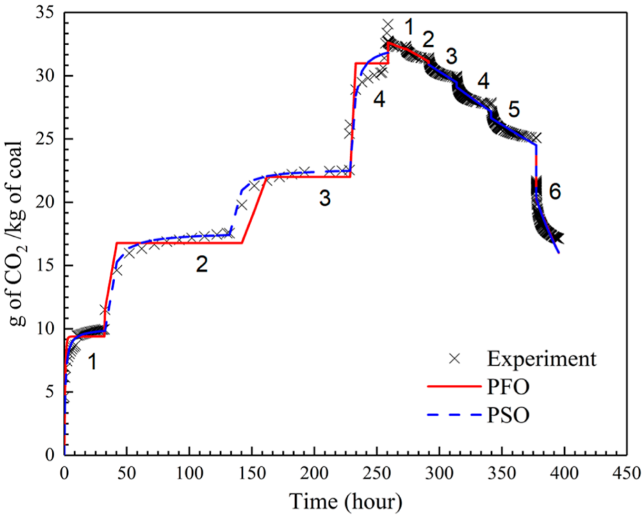

Figure 4. CO_2 adsorption−desorption kinetics data fit to PFO and PSO models. Sample EMB1 and experimental condition EXP1 (the numbers in the plot represent the injection pressure stages; Table 3).

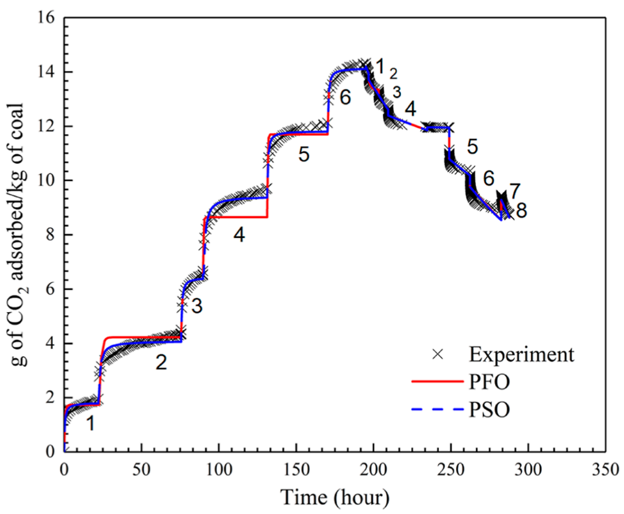

Figure 5. CO_2 adsorption−desorption kinetics data fit to PFO and PSO models. Sample EMB1 and experimental condition EXP2 (the numbers in the plot represent the injection pressure stages; Table 4).

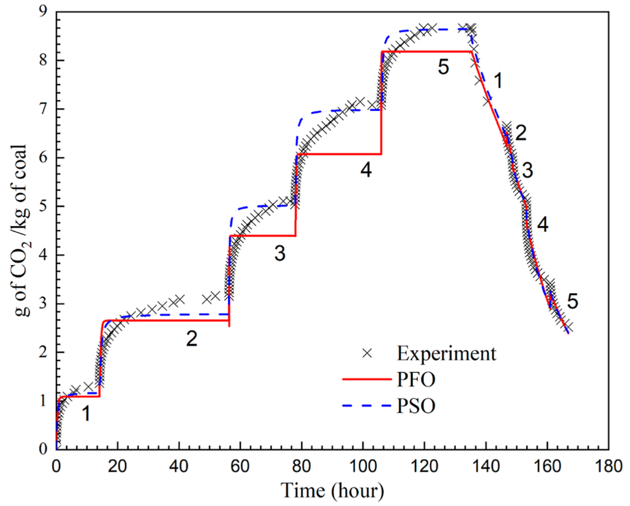

Figure 6. CO_2 adsorption−desorption kinetics data fit to PFO and PSO models. Sample EMB2 and experimental condition EXP3 (the numbers in the plot represent the injection pressure stages; Table 5).

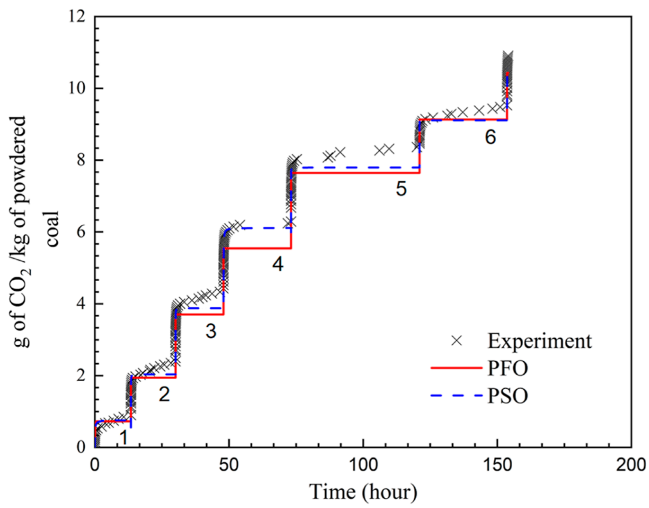

Figure 7. CO_2 adsorption kinetics data fit to PFO and PSO models. Powdered sample and experimental condition EXP4 (the numbers in the plot represent the injection pressure stages; Table 6).

CO_2 adsorption on coal. Furthermore, the PSO kinetic model analysis was used to predict CO_2 adsorption on solid adsorbents, as well as the previously observed relationship between the PSO rate constant, k_{a2}, and the diffusion coefficient of adsorbent microspheres in the unipore model, which says that CO_2 adsorption on coal is controlled by pore diffusion.[30−35]

At higher pressures (up to 4.5 MPa; Figure 4, Table 3), the inconsistent relationship between the equilibrium pressure and the kinetic rate constant (k_{a2}) of the PSO model indicates that the heterogeneous nature of the coal samples has an effect on adsorption and that bulk pore diffusion, surface physical adsorption, and pore filling occur first, followed by slow surface interactions. For example, as the equilibrium pressure increased from 0.63 to 2.5 MPa, the PSO rate constant (k_{a2}) increased (from 0.21 to 0.32 kg/g h). At 3.6 MPa, the rate constant fluctuated to 0.31 kg/g h. The pressure independence of PSO parameters (k_{a2} and q_{ae}) at lower pressures (0.5 MPa; Tables 4 and 5; Figures 5 and 6) indicates that the varying sizes of the pores in the coal have an effect on the adsorption process and that different mechanisms determine the rate of CO_2 adsorption on intact coal samples. The higher rate constants (k_{a2}; Tables 4 and 5) observed in low pressure adsorption experiments indicate that monolayer adsorption/pore filling occurs initially, followed by multilayer or pore condensation.[30] As previous studies aimed to achieve higher density and higher adsorption at supercritical injection, no detailed comparative adsorption kinetic data for large intact samples at the given low temperature and pressure ranges has been published. As a result, the rate constant values presented in the current study for the intact bituminous coal samples had to be thoroughly evaluated.

Compared to the equilibrium times of lower pressure (Table 4; EXP2) experiments of EMB1 with those of high-pressure experiments (Table 3; EXP1), it took longer to attain equilibrium at higher pressures. The equilibrium times of the individual pressure stages show that the adsorption was a slow process in the low-pressure experiments. For example, to adsorb 10.06 g of CO_2/kg of coal, it took 36 h to reach

https://doi.org/10.1021/acs.energyfuels.2c01426
Energy Fuels 2022, 36, 8360−8370

Table 3. PFO and PSO Model Parameters Obtained from Fitting EMB1 EXP1 Experimental Data[a]

pressure step-up stage no.				PFO				PSO			
adsorption	pressure A (MPa)	pressure B (MPa)	equilibrium time (h)	k_{a1} (h^{-1})	q_{e1} (g/kg)	R^2	SEOE	k_{a2} (kg/g h)	q_{e2} (g/kg)	R^2	SEOE
1	1.03	0.63	32	1.5	9.39	0.99	0.67	0.21	9.81	0.89	0.41
2	2.02	1.43	96	2.32	16.8	0.99	0.77	0.23	16.9	0.91	0.67
3	3.02	2.50	31	4.2	22	0.99	0.98	0.32	21.99	0.81	0.68
4	4.05	3.60	14	3.71	30.98	0.99	1.46	0.31	31.2	0.66	1.4
pressure step-up stage no.				PFO				PSO			
desorption	pressure A (MPa)	pressure B (MPa)	equilibrium time (h)	k_{d1} (h^{-1})	q_{d1} (g/kg)	R^2	SEOE	k_{d2} (kg/g h)	q_{e2} (g/kg)	R^2	SEOE
1	3.08	3.21	14	0.001	32.6	0.76	0.08	3.7×10^{-5}	32.62	0.76	0.08
2	2.55	2.73	18	0.001	32.1	0.18	0.58	5.5×10^{-5}	32.2	0.18	0.58
3	2.01	2.23	22	0.002	30.9	0.79	0.199	6.9×10^{-5}	30.88	0.78	0.199
4	1.5	1.75	27	0.002	29	0.68	0.335	8.9×10^{-5}	29.1	0.69	0.332
5	1.02	1.31	36	0.002	26	0.74	0.353	0.0024	26.66	0.74	0.348
6	0.051	0.085	17	0.013	20	0.72	0.79	0.00073	20.27	0.75	0.76

[a]A = injection pressure in RC. B = equilibrium pressure in (RC + SC) referring to the pressure at A.

Table 4. PFO and PSO Model Parameters Obtained from Fitting EMB1 EXP2 Experimental Data[a]

pressure step-up stage no.				PFO				PSO			
adsorption	pressure A (MPa)	pressure B (MPa)	equilibrium time (h)	k_{a1} (h^{-1})	q_{e1} (g/kg)	R^2	SEOE	k_{a2} (kg/g h)	q_{e2} (g/kg)	R^2	SEOE
1	0.14	0.035	22	1.83	1.73	0.99	0.14	1.47	1.81	0.99	0.097
2	0.22	0.09	53	0.86	4.22	0.99	0.39	0.54	4.09	0.77	0.21
3	0.32	0.19	14	3.71	6.27	0.97	1.04	1.17	6.43	0.58	0.41
4	0.45	0.28	41	5.02	8.64	0.98	1.21	0.37	9.43	0.86	0.27
5	0.53	0.39	39	4.53	11.68	0.99	0.29	1.12	11.81	0.6	0.32
6	0.64	0.51	24	4.47	13.99	0.99	0.28	1.1	14.14	0.47	0.38
pressure step-up stage no.				PFO				PSO			
desorption	pressure A (MPa)	pressure B (MPa)	equilibrium time (h)	k_{d1} (h^{-1})	q_{d1} (g/kg)	R^2	SEOE	k_{d2} (kg/g h)	q_{e2} (g/kg)	R^2	SEOE
1	0.41	0.44	6.5	0.01	14.2	0.77	0.046	0.0007	14.2	0.77	0.046
2	0.31	0.37	6	0.006	13.71	0.66	0.103	0.0005	13.71	0.67	0.102
3	0.26	0.31	25	0.007	13.14	0.73	0.094	0.0005	13.14	0.75	0.093
4	0.2	0.25	14	0.002	12.39	0.5	0.145	0.00015	12.39	0.5	0.145
5	0.15	0.21	13	6.2×10^{-6}	11.95	0.71	0.002	5.15×10^{-6}	11.95	0.54	0.002
6	0.1	0.16	20	0.004	10.78	0.54	0.142	0.0004	10.78	0.55	0.014
7	0.063	0.094	20	0.007	9.76	0.59	0.23	0.0007	9.77	0.6	0.23
8	0	0.03	5	0.014	9.28	0.78	0.103	0.002	9.28	0.78	0.102

[a]A = injection pressure in RC. B = equilibrium pressure in (RC + SC) for the injection pressure A.

equilibrium pressure of 0.63 MPa (stage no. 1, Table 3) in high injection pressure experiments. To adsorb a similar amount of CO_2 (9.43 g of CO_2/kg of coal), the EMB1 sample required 130 h of cumulative equilibrium time (stage nos. 1 to 4; Table 4) at low pressure injections (up to 0.5 MPa). The results from the current study indicate that the longer equilibrium times and small step-up injection pressures can yield maximum adsorption capacity at low pressure injections (up to 0.5 MPa; Figures 5 and 6; Tables 4 and 5) in shallow level bituminous coal seams.

Equilibrium times of desorption kinetics show that the equilibrium was attained faster than the adsorption pressure step up kinetic experiments. However, the amount remaining adsorbed was greater than that of the corresponding equilibrium conditions of the adsorption because all the adsorbed CO_2 was not readily desorbed, or the process was not reversible, which further explains the better fit of the second-order kinetic model. The significant amount of residual CO_2 trapped in the coal samples (Figures 4−7) was attributed to the pore trapping mechanisms such as pore blockage, gas cavitation, adsorption induced deformation, and pore network effect or ink bottle effect.[58−60] The results in Figure 4 show that 17 g of CO_2/kg of coal remained in the EMB1 coal core at the end of the desorption experiments. Similar CO_2 entrapment was observed during the lower pressure EXP2 and EXP3 tests on the intact EMB1 and EMB2 coal cores (Figures 5 and 6). The residual amount of CO_2 retained in the EMB1 and EMB2 samples, during low injection pressure, was about 8 g of CO_2/kg of coal (up to 0.64 MPa injection pressure) and 2.52 g of CO_2/kg of coal (up to 0.52 MPa injection pressure), respectively. This means that small increments in injection pressures can result in an increased amount of residual CO_2

https://doi.org/10.1021/acs.energyfuels.2c01426
Energy Fuels 2022, 36, 8360−8370

Table 5. PFO and PSO Model Parameters Obtained from Fitting EMB2 EXP3 Experimental Data[a]

pressure step-up stage no.				PFO				PSO			
adsorption	pressure A (MPa)	pressure B (MPa)	equilibrium time (h)	k_{a1} (h^{-1})	q_{e1} (g/kg)	R^2	SEOE	k_{a2} (kg/g h)	q_{e2} (g/kg)	R^2	SEOE
1	0.13	0.058	14	3.0	1.09	0.76	0.17	3.57	1.19	0.86	0.12
2	0.21	0.12	42	3.57	2.65	0.65	0.32	12.18	2.79	0.81	0.23
3	0.32	0.21	21	14.74	4.39	0.36	0.49	8.98	5.03	0.3	0.5
4	0.41	0.3	28	7.27	6.07	0.42	0.52	14.7	7	0.47	0.46
5	0.52	0.40	29	36.17	8.18	0.15	0.52	10.77	8.66	0.69	0.31
pressure step-up stage no.				PFO				PSO			
desorption	pressure A (MPa)	pressure B (MPa)	equilibrium time (h)	k_{d1} (h^{-1})	q_{d1} (g/kg)	R^2	SEOE	k_{d2} (kg/g h)	q_{e2} (g/kg)	R^2	SEOE
1	0.33	0.37	11.5	0.025	7.98	0.80	0.30	0.0004	8.43	0.91	0.2
2	0.24	0.3	1.8	0.053	6.12	0.88	0.07	0.009	6.52	0.88	0.07
3	0.15	0.23	4.5	0.036	5.42	0.98	0.1	0.007	5.82	0.88	0.1
4	0.021	0.13	7.5	0.068	4.29	0.76	0.34	0.02	4.7	0.8	0.22
5	0.06	0.08	5.5	0.06	2.87	0.99	0.08	0.024	3.26	0.92	0.08

[a]A = injection pressure in RC. B = equilibrium pressure in (RC + SC) for the injection pressure A.

Table 6. PFO and PSO Model Parameters Obtained from Fitting Powdered Coal EXP3 Experimental Data[a]

pressure step-up stage no.				PFO				PSO			
adsorption	pressure A (MPa)	pressure B (MPa)	equilibrium time (h)	k_{a1}	q_{ae}	R^2	SEOE	k_{a2}	q_{ae}	R^2	SEOE
1	0.11	0.042	13.4	10.10	0.73	0.83	0.12	16.23	0.76	0.89	0.09
2	0.20	0.095	16.64	90.47	1.94	0.59	0.26	66.83	2.04	0.75	0.2
3	0.31	0.17	17.88	130.87	3.75	0.49	0.39	70.51	3.88	0.76	0.27
4	0.42	0.27	25.13	458.37	5.54	0.22	0.46	14.24	6.11	0.99	0.06
5	0.51	0.36	47.92	649.36	7.64	0.15	0.45	149.45	7.79	0.59	0.34
6	0.52	0.43	32.62	967	9.06	0.27	0.27	397	9.1	0.45	0.28

[a]A = injection pressure in RC. B = equilibrium pressure in (RC + SC) for the injection pressure A.

retained in the micropore channels of bituminous coals, independent of sample sizes used in the experiments. Therefore, residual CO_2 in intact cores is correlated with the equilibrium pressures, indicating the small amount of residual was achieved for EMB2 as the pressure was not sufficient for the CO_2 to enter the ultra-nanopores. This further strengthens the assumptions of the PFO and PSO models of surface interaction and pore diffusion and condensation. Overall, the analysis indicates that CO_2 adsorption on bituminous EMB coal is controlled by the pore diffusion process in the initial stages and surface interaction takes over. To compare the desorption kinetics results obtained from PFO and PSO models (Tables 3−5), there are no published desorption kinetics data. Therefore, detailed desorption kinetics studies needed to be studied further to ascertain the reversibility of CO_2 adsorption.

The powder sample showed an increasing trend in equilibrium times (Table 6), with the equilibrium pressure demonstrating that large, exposed polarized sites cause surface interaction mechanisms to take over following pore diffusion. The active sites in bituminous coals are created by functional groups and carbon-containing groups, which become more exposed when coal is pulverized.[26,61] For the powdered sample experimental data, the SEOE values show that the PSO model fit better than the PFO model, supporting the above-mentioned interpretation that surface interaction is the slowest rate-determining step rather than physical adsorption and diffusion processes (Figure 7; Table 6). A similar type of experiment conducted by Gabruś et al. (2021)[34] showed significantly higher k_{a1} and k_{a2} values than the current study (k_{ad1} was in the range of 1.6×10^6 to 1.0×10^6 h^{-1} and k_{ad2} was in the range of 5.7×10^6 to 12×10^6 h^{-1}). However, the present study intends to allow the equilibrium to occur for each pressure step, whereas in the previous experiments the equilibrium values were reported for only 24 h (for pressure ranging from 0.5 to 6.4 MPa).

Despite the increased surface area of the powdered samples, the intact samples showed similar equilibrium adsorbed amount (q_e) values obtained for the powdered samples at comparable pressure and temperature conditions. The q_e values were 11.68 g/kg (at 0.53 MPa) and 7.58 g/kg (at 0.52 MPa) for the intact EMB1 and EMB2 samples, whereas the powdered sample showed 9.06 g/kg (at 0.52 MPa). These results indicate the influence of channel-like pores on the high-density CO_2 (liquid like) adsorption in intact samples. These pores will be lost or modified when the samples are powdered, and less density gas phase adsorption occurs in the large surface area exposed.

3.2. Bangham Model for the Pore Diffusion-Controlled Adsorption Process. To ascertain the pore diffusion theory, the experimental data set was fitted into the Bangham model. The Bangham model fitting, shown in Figure 8, predicts that the q_e values are closely matched to those calculated using the PSO and the PFO model. Moreover, for PFO and PSO the data needed to be fitted segmentally for the specific equilibrium pressure stages, whereas the entire data set

https://doi.org/10.1021/acs.energyfuels.2c01426
Energy Fuels 2022, 36, 8360−8370

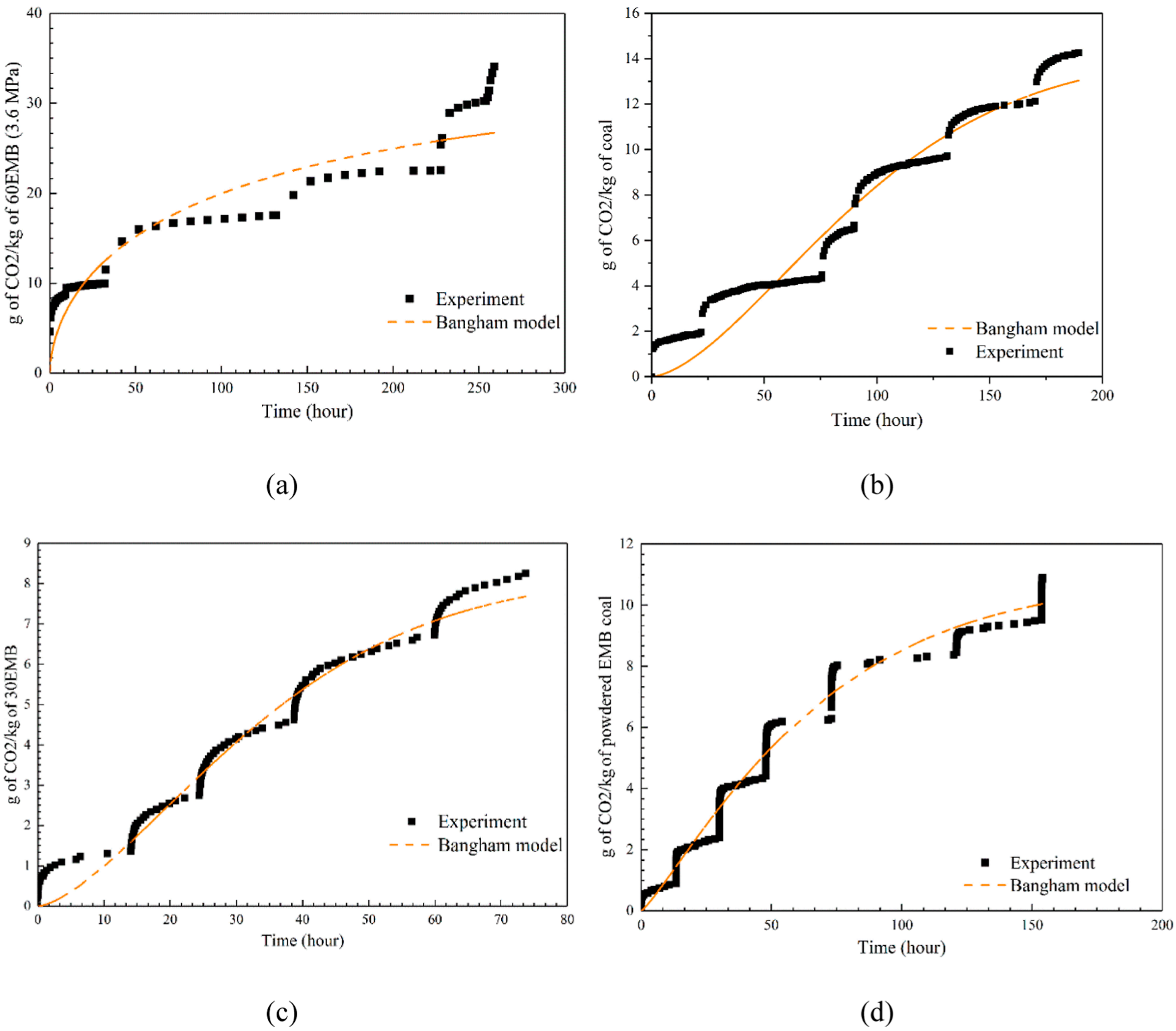

Figure 8. CO_2 adsorption−desorption kinetics data fitted to the Bangham pore diffusion model. (a) Sample EMB1, experimental condition EXP1 and (b) EXP2; (c) sample EMB2, experimental condition EXP3; and (d) powdered sample and experimental condition EXP4.

has been (all the stages) used in the nonlinear fitting of the Bangham model (Figure 8). The model parameters and the coefficient of determination (R^2) values listed in Table 7 show that the CO_2 adsorption on bituminous EMB coal is pore diffusion controlled at a pressure range of 0.5 to 4.5 MPa at a temperature of 298.15 K.

The pressure dependency of the adsorption kinetic model parameters (n and k_b) and the coefficient of determination (R^2) values show that bulk pore diffusion is not the only the rate-determining factor. At lower pressure experiments, the parameters n and k_b are greater than at higher-pressure experiments, implying that the pore diffusion is the rate-determining step at lower pressures and the surface interaction is the rate-determining step at higher equilibrium pressures. The coefficient of determination values complies with the observations as the value observed for high pressure experiment (up to 3.6 MPa) was 0.87 and which are smaller than that of low-pressure (up to 0.5 MPa) adsorption experiments of same sized EMB1 coal (R^2 = 0.94). Much lower equilibrium pressure experiments with the EMB2 sample (up to 0.4 MPa) were in good agreement with the model (R^2 = 0.98), underscoring that the pore diffusion is the predominate rate-determining factor at lower pressure and surface interaction takes over at higher pressures.[62] The standard error of estimate was correlated with the coefficient of determination (R^2) values. The powdered samples showed a similar trend to the pore diffusion model data fitting (Figure 8d). The better fit in the PSO model for powdered materials (Figure 7 and Table 6) and longer equilibrium durations imply that the rate

Table 7. Fitting Parameters of the Bangham Pore Diffusion Model

experiment	sample	k_b (h^{-1})	n	SEOE	R^2
EXP1	EMB1	0.061	0.58	2.94	0.87
EXP2		0.0006	1.6	0.98	0.94
EXP3	EMB2	0.004	1.52	0.35	0.98
EXP4	powder	0.007	1.18	0.45	0.98

https://doi.org/10.1021/acs.energyfuels.2c01426
Energy Fuels 2022, 36, 8360−8370

controlling process is CO_2 interaction with polarized sites, followed by early pore diffusion and condensation.

4. CONCLUSIONS

This study presented extensive data from adsorption–desorption kinetics for injection pressures of up to 0.5 MPa in the context of injecting CO_2 into shallow level coal seams for the first time. The powdered samples took longer to reach equilibrium, indicating exposed surface sites that are unlikely to be present if the coal is intact. At the same corresponding equilibrium pressures, the comparable equilibrium amount of CO_2 adsorbed on the intact and powdered samples indicated the importance of conducting experiments with large intact samples.

The PSO model fitted the experimental data well for both adsorption and desorption kinetics, implying that pore diffusion and surface interaction are the rate-determining steps. The cumulative experimental data fitting to the Bangham diffusion model supported the idea that pore diffusion is the rate-determining step in the CO_2 adsorption process on bituminous EMB coal at lower pressures.

The current study established detailed CO_2 desorption kinetics from intact coal samples for perhaps the first time, and the data fitted into the modified PFO and PSO models. The data from desorption kinetics confirm the prediction by demonstrating the pore trapping capabilities. The amount of residual CO_2 retained in the coal sample at the end of the desorption tests demonstrates the pore trapping capabilities of the bituminous coal sample. The amount of CO_2 trapped was proportional to the equilibrium pressure.

In broad sense, the adsorption–desorption kinetics experiments provided insights into rate-determining mechanism, reversibility of CO_2 adsorption, or pore entrapment of CO_2 at the low-pressure injection in shallow level bituminous coal seams.

AUTHOR INFORMATION

Corresponding Author

Sivachidambaram Sadasivam – *Geoenvironmental Research Centre (GRC), School of Engineering, Cardiff University, Cardiff CF24 3AA, U.K.;* orcid.org/0000-0002-2305-0292; Email: sadasivams@cardiff.ac.uk

Authors

Shakil Masum – *Geoenvironmental Research Centre (GRC), School of Engineering, Cardiff University, Cardiff CF24 3AA, U.K.*

Min Chen – *Geoenvironmental Research Centre (GRC), School of Engineering, Cardiff University, Cardiff CF24 3AA, U.K.;* orcid.org/0000-0003-0809-7436

Kamil Stańczyk – *Główny Instytut Górnictwa (Central Mining Institute), Katowice 40-166, Poland*

Hywel Thomas – *Geoenvironmental Research Centre (GRC), School of Engineering, Cardiff University, Cardiff CF24 3AA, U.K.*

Complete contact information is available at: https://pubs.acs.org/10.1021/acs.energyfuels.2c01426

Notes

The authors declare no competing financial interest.

ACKNOWLEDGMENTS

The research was conducted as part of the "Establishing a Research Observatory to Unlock European Coal Seams for Carbon Dioxide Storage (ROCCS)" project. The ROCCS project has received funding from the Research Fund for Coal and Steel under grant agreement no. 899336. The ROCCS project is also co-financed by the program of the Minister of Science and Higher Education, Poland, entitled "PMW" in the years 2020–2023; agreement no. 5144/FBWiS/2020/2. The financial support is gratefully acknowledged. The authors would like to thank Anthony Oldroyd, Technician, School of Earth Sciences, Cardiff University for the technical support. Dr. Ramesh Kannan, Department of Civil Engineering, Indian Institute of Technology, Chennai, India is thanked for their support in X-CT analysis. CT data were obtained at the XTM Facility, Palaeobiology Research Group, University of Bristol and we thank Dr. Liz Martin-Silverstone for acquiring the data.

REFERENCES

(1) Le Quéré, C.; Moriarty, R.; Andrew, R. M.; Canadell, J. G.; Sitch, S.; Korsbakken, J. I.; Friedlingstein, P.; Peters, G. P.; Andres, R. J.; Boden, T. A.; et al. Global Carbon Budget 2015. *Earth Syst. Sci. Data* **2015**, *7*, 349–396.

(2) IPCC. *Global Warming of 1.5 °C. An IPCC Special Report on the Impacts of Global Warming of 1.5 °C above Pre-industrial Levels and Related Global Greenhouse Gas Emission Pathways, in the Context of Strengthening the Global Response to the Threat of Climate Change, Sustainable Development, and Efforts to Eradicate Poverty*; Masson-Delmotte, V., Zhai, P., Pörtner, H.-O., Roberts, D., Skea, J., Shukla, P. R., Pirani, A., Moufouma-Okia, W., Péan, C., Pidcock, R., etal, Eds., 2018.

(3) Fleurbaey, M.; Kartha, S.; Bolwig, S.; Chee, Y. L.; Chen, Y.; Corbera, E.; Lecocq, F.; Lutz, W.; et al. Chapter 4—Sustainable development and equity. In *Climate Change 2014: Mitigation of Climate Change. IPCC Working Group III Contribution to AR5*; Cambridge University Press: Cambridge, 2014.

(4) Kolstad, C.; Urama, K.; Broome, J.; Bruvoll, A.; Cariño Olvera, M.; Fullerton, D.; Gollier, C.; Hanemann, W. M.; Hassan, R.; Jotzo, F.; et al. Social, Economic and Ethical Concepts and Methods. In *Climate Change 2014: Mitigation of Climate Change. Contribution of Working Group III to the Fifth Assessment Report of the Intergovernmental Panel on Climate Change*; Edenhofer, O., Pichs-Madruga, R., Sokona, Y., Farahani, E., Kadner, S., Seyboth, K., Adler, A., Baum, I., Brunner, S., Eickemeier, P., etal, Eds.; Cambridge University Press: New York, NY, USA, 2014.

(5) Global CCS Institute. *The Global Status of CCS: 2016 Summary Report*, Australia, 2016.

(6) COP26. 2021, https://ukcop26.org/cop26-goals/ (accessed June 20, 2022).

(7) Bachu, S. 2—Screening and selection criteria, and characterisation techniques for the geological sequestration of carbon dioxide (CO2). In *Developments and Innovation in Carbon Dioxide (CO2) Capture and Storage Technology*; Mercedes Maroto-Valer, M., Ed.; Woodhead Publishing Series in Energy; Woodhead Publishing, 2010; Vol. *2*, pp 27–56. https://www.sciencedirect.com/science/article/pii/B9781845697976500023.

(8) Laubach, S. E.; Marrett, R. A.; Olson, J. E.; Scott, A. R. Characteristics and origins of coal cleat: A review. *Int. J. Coal Geol.* **1998**, *35*, 175–207.

(9) White, C. M.; Smith, D. H.; Jones, K. L.; Goodman, A. L.; Jikich, S. A.; LaCount, R. B.; DuBose, S. B.; Ozdemir, E.; Morsi, B. I.; Schroeder, K. T. Sequestration of carbon dioxide in coal with enhanced coalbed methane recovery—A review. *Energy Fuels* **2005**, *19*, 659–724.

(10) Majewska, Z.; Majewski, S.; Ziętek, J.; Ceglarska-Stefańska, G. Volumetric strain induced in medium-rank coal by sorption of carbon dioxide, methane and their mixture. In *Carbon Sequestration: Methods,*

Modeling and Impacts; Hoch, E., Crunwald, S., Eds.; Nova Publishers: New York, 2010; Chapter 4.

(11) Strąpoć, D.; Mastalerz, M.; Schimmelmann, A.; Eble, C. Biogenic and thermogenic coalbed gas in the Illinois Basin: insight from compound-specific carbon isotopic ratios. In *Proceedings of the 22nd International Meeting on Organic Geochemistry*, Seville, Spain, Sept 12−16, 2005; Vol. *1*, pp 113−114.

(12) Jones, E. J. P.; Voytek, M. A.; Warwick, P. D.; Corum, M. D.; Cohn, A.; Bunnell, J. E.; Clark, A. C.; Orem, W. H. Bioassay for estimating the biogenic methane-generating potential of coal samples. *Int. J. Coal Geol.* **2008**, *76*, 138−150.

(13) Merkel, A.; Gensterblum, Y.; Krooss, B. M.; Amann, A. Competitive sorption of CH4, CO2 and H2O on natural coals of different rank. *Int. J. Coal Geol.* **2015**, *150−151*, 181−192.

(14) Sams, W. N.; Bromhal, G.; Jikich, S.; Ertekin, T.; Smith, D. H. Field-Project Designs for Carbon Dioxide Sequestration and Enhanced Coalbed Methane Production. *Energy Fuels* **2005**, *19*, 2287−2297.

(15) Vangkilde-Pedersen, T.; Anthonsen, K. L.; Smith, N.; Kirk, K.; Neele, F.; van der Meer, B.; Le Gallo, Y.; Bossie-Codreanu, D.; Wojcicki, A.; Le Nindre, Y.-M.; Hendriks, C.; Dalhoff, F.; Christensen, N. P.; et al. Assessing European capacity for geological storage of carbon dioxide−the EU GeoCapacity project. *Energy Procedia* **2009**, *1*, 2663−2670.

(16) Masoudian, M. S. Multiphysics of carbon dioxide sequestration in coalbeds: A review with a focus on geomechanical characteristics of coal. *J. Rock Mech. Geotech. Eng.* **2016**, *8*, 93−112.

(17) Krooss, B. M.; van Bergen, F.; Gensterblum, Y.; Siemons, N.; Pagnier, H. J. M.; David, P. High-pressure methane and carbon dioxide adsorption on dry and moisture-equilibrated. Pennsylvanian coals. *Int. J. Coal Geol.* **2002**, *51*, 69−92.

(18) Fitzgerald, J. E.; Pan, Z.; Sudibandriyo, M.; Robinson, R. L.; Gasem, K. A. M.; Reeves, S. Adsorption of methane, nitrogen, carbon dioxide and their mixtures on wet Tiffany coal. *Fuel* **2005**, *84*, 2351−2363.

(19) Siemons, N.; Busch, A. Measurement and interpretation of supercritical CO2 sorption on various coals. *Int. J. Coal Geol.* **2007**, *69*, 229−242.

(20) Lee, H.-H.; Kim, H.-J.; Shi, Y.; Keffer, D.; Lee, C.-H. Competitive adsorption of CO2/CH4 mixture on dry and wet coal from subcritical to supercritical conditions. *Chem. Eng. J.* **2013**, *230*, 93−101.

(21) Zagorščak, R.; Thomas, H. R. High-pressure CO2 excess sorption measurements on powdered and core samples of high-rank coals from different depths and locations of the South Wales Coalfield. *Energy Fuels* **2019**, *33*, 6515−6526.

(22) Busch, A.; Gensterblum, Y.; Krooss, B. M. Methane and CO2 sorption and desorption measurements on dry Argonne premium coals: pure components and mixtures. *Int. J. Coal Geol.* **2003**, *55*, 205−224.

(23) Li, D.; Liu, Q.; Weniger, P.; Gensterblum, Y.; Busch, A.; Krooss, B. M. High-pressure sorption isotherms and sorption kinetics of CH4 and CO2 on coals. *Fuel* **2010**, *89*, 569−580.

(24) Siemons, N.; Busch, A. Measurement and interpretation of supercritical CO2 sorption on various coals. *Int. J. Coal Geol.* **2007**, *69*, 229−242.

(25) Day, S.; Fry, R.; Sakurovs, R. Swelling of Australian coals in supercritical CO2. *Int. J. Coal Geol.* **2008**, *74*, 41−52.

(26) Mastalerz, M.; Gluskoter, H.; Rupp, J. Carbon dioxide and methane sorption in high volatile bituminous coals from Indiana, USA. *Int. J. Coal Geol.* **2004**, *60*, 43−55.

(27) Chen, S.; Tang, D.; Tao, S.; Xu, H.; Zhao, J.; Fu, H.; Ren, P. In-situ stress, stress-dependent permeability, pore pressure and gas-bearing system in multiple coal seams in the Panguan area, western Guizhou, China. *J. Nat. Gas Sci. Eng.* **2018**, *49*, 110−122.

(28) Pone, J. D. N.; Halleck, P. M.; Mathews, J. P. Sorption Capacity and Sorption Kinetic Measurements of CO2 and CH4 in Confined and Unconfined Bituminous Coal. *Energy Fuels* **2009**, *23*, 4688−4695.

(29) Espinoza, D. N.; Vandamme, M.; Pereira, J.-M.; Dangla, P.; Vidal-Gilbert, S. Measurement and modeling of adsorptive-poromechanical properties of bituminous coal cores exposed to CO2: adsorption, swelling strains, swelling stresses and impact on fracture permeability. *Int. J. Coal Geol.* **2014**, *134*, 80−95.

(30) Tang, X.; Ripepi, N.; Gilliland, E. Isothermal adsorption kinetics properties of carbon dioxide in crushed coal. *Greenhouse Gases: Sci. Technol.* **2016**, *6*, 260−274.

(31) Qin, C.; Jiang, Y.; Zuo, S.; Chen, S.; Xiao, S.; Liu, Z. Investigation of adsorption kinetics of CH4 and CO2 on shale exposure to supercritical CO2. *Energy* **2021**, *236*, 121410.

(32) Wang, J.; Li, M.; Lu, P.; Ning, P.; Wang, Q. Kinetic study of CO_2 capture on ternary nitrates modified MgO with different precursor and morphology. *Chem. Eng. J.* **2020**, *392*, 123752.

(33) Bhatta, L. K. G.; Subramanyam, S.; Chengala, M. D.; Bhatta, U. M.; Venkatesh, K. Low-temperature CO_2 adsorption on Titania nanotubes (TNTs). *Surf. Interfaces* **2017**, *8*, 158−162.

(34) Gabruś, E.; Wojtacha-Rychter, K.; Aleksandrzak, T.; Smoliński, A.; Król, M. The feasibility of CO_2 emission reduction by adsorptive storage on Polish hard coals in the Upper Silesia Coal Basin: An experimental and modeling study of equilibrium, kinetics and thermodynamics. *Sci. Total Environ.* **2021**, *796*, 149064.

(35) Shi, F.; Wei, Z.; Zhang, D.; Huang, G. Isotherms and kinetics of deformation of coal during carbon dioxide sequestration and their relationship to sorption. *Int. J. Coal Geol.* **2020**, *231*, 103606.

(36) Bangham, D. H.; Burt, F. P. The Behavior of Gases in Contact with Glass Surfaces. *Proc. R. Soc. London, Ser. A* **1924**, *105*, 481−488.

(37) Bangham, D. H.; Burt, F. P. Sorption of Ammonia and Carbon Dioxide by Glass. *J. Phys. Chem. A* **2002**, *29*, 113−129.

(38) Bangham, D. H.; Sever, W. XCIII. *An experimental investigation of the dynamical equation of the process of gas-sorption. London, Edinburgh Dublin Philos. Mag. J. Sci.* **1925**, *49*, 935−944.

(39) Saghafi, A.; Faiz, M.; Roberts, D. CO_2 storage and gas diffusivity properties of coals from Sydney Basin, Australia. *Int. J. Coal Geol.* **2007**, *70*, 240−254.

(40) Pirzada, M. A.; Zoorabadi, M.; Ramandi, H. L.; Canbulat, I.; Roshan, H. CO2 sorption induced damage in coals in unconfined and confined stress states: A micrometer to core scale investigation. *Int. J. Coal Geol.* **2018**, *198*, 167−176.

(41) Mosleh, M. H.; Turner, M.; Sedighi, M.; Vardon, P. J. Carbon dioxide flow and interactions in a high rank coal: Permeability evolution and reversibility of reactive processes. *Int. J. Greenhouse Gas Control* **2018**, *70*, 57−67.

(42) Ozdemir, E.; Morsi, B. I.; Schroeder, K. Importance of volume effects to adsorption isotherms of carbon dioxide on coals. *Langmuir* **2003**, *19*, 9764−9773.

(43) Harpalani, S.; Chen, G. Estimation of changes in fracture porosity of coal with gas emission. *Fuel* **1995**, *74*, 1491−1498.

(44) George, J. D.; Barakat, M. A. The change in effective stress associated with shrinkage from gas desorption in coal. *Int. J. Coal Geol.* **2001**, *45*, 105−113.

(45) Zutshi, A.; Harpalani, S. Matrix swelling with CO2 injection in a ABM reservoir and its impact on permeability of coal. *Proceedings of the 2004 International Coalbed Methane Symposium*, Tuscaloosa, AL, 2004; p 46.

(46) Mosleh, M. D. An Experimental Investigation of Flow and Reaction Processes During Gas Storage and Displacement in Coal. Ph.D. Thesis, Cardiff University, 2014.

(47) DIN method: DIN 51913:2001, testing of carbon materials—determination of density by gas pycnometer (volumetric) using helium as the measuring gas−solid materials prepared by Arbeitsausschuß NMP 281, test methods for carbon and graphite.

(48) Keller, U.; Staudt, R. *Gas Adsorption Equilibria: Experimental Methods and Adsorptive Isotherms (Universität Siegen)*; Springer: New York, 2005.

(49) Ruthven, D. M. *Principles of Adsorption and Adsorption Processes*; Wiley: New York, 1984.

(50) Rouquerol, F.; Rouquerol, J.; Sing, K. Chapter 1—Introduction. In *Adsorption by Powders and Porous Solids*;

https://doi.org/10.1021/acs.energyfuels.2c01426
Energy Fuels 2022, 36, 8360−8370

Rouquerol, F., Rouquerol, J., Sing, K., Rouquerol, F., Rouquerol, J., Sing, K., Eds.; Academic Press, 2013; pp 1−26.
(51) Myers, A. L.; Monson, P. A. Physical adsorption of gases: the case for absolute adsorption as the basis for thermodynamic analysis. *Adsorption* **2014**, *20*, 591−622.
(52) Toth, J. *Adsorption: Theory, Modeling, and Analysis*; Surfactant Science Series; Marcel Dekker, 2002; Vol. *107* (50), pp 971−983.
(53) Elliott, J. R.; Lira, C. T. *Introductory Chemical Engineering Thermodynamics*; Prentice Hall PTR: Upper Saddle River, NJ, 2012.
(54) Guo, J.; Zhai, Z.; Wang, L.; Wang, Z.; Wu, J.; Zhang, B.; Zhang, J. Dynamic and thermodynamic mechanisms of TFA adsorption by particulate matter. *Environ. Pollut.* **2017**, *225*, 175−183.
(55) Hu, A.; Zhang, Y.; Xiong, P.; Yang, Y.; Liu, Z. Kinetic characteristics and modeling comparison of methane adsorption on gas shale. *Energy Sources, Part A* **2020**, DOI: 10.1080/15567036.2020.1849461.
(56) Njikam, E.; Schiewer, S. Optimization and kinetic modeling of cadmium desorption from citrus peels: A process for biosorbent regeneration. *J. Hazard. Mater.* **2012**, *213*−*214*, 242−248.
(57) Swan, E.; Urquhart, A. R. Adsorption Equations. *J. Phys. Chem.* **1927**, *31*, 251−276.
(58) Wang, K.; Wang, G.; Ren, T.; Cheng, Y. Methane and CO_2 Sorption Hysteresis on Coal: A Critical Review. *Int. J. Coal Geol.* **2014**, *132*, 60−80.
(59) Wang, G. D.; Ren, T. X.; Qi, Q. X.; Wang, K.; Zhang, L. Mechanism of Adsorption-Desorption Hysteresis and its Influence on Deep CBM Recovery. *J. China Coal Soc.* **2016**, *41*, 49−56.
(60) Ren, J.; Weng, H.; Li, B.; Chen, F.; Liu, J.; Song, Z. The Influence Mechanism of Pore Structure of Tectonically Deformed Coal on the Adsorption and Desorption Hysteresis. *Front. Earth Sci.* **2022**, *10*, 841353.
(61) Nishino, J. Adsorption of water vapor and carbon dioxide at carboxylic functional groups on the surface of coal. *Fuel* **2001**, *80*, 757−764.
(62) Tütem, E.; Apak, R.; Ünal, C. F. Adsorptive removal of chlorophenols from water by bituminous shale. *Water Res.* **1998**, *32*, 2315−2324.

https://doi.org/10.1021/acs.energyfuels.2c01426
Energy Fuels 2022, 36, 8360−8370